Vacuum 176 (2020) 109167

Contents lists available at ScienceDirect

Vacuum

journal homepage: http://www.elsevier.com/locate/vacuum

A comprehensive study of molybdenum boats behavior during service life for continuous thermal evaporation technique, used in thin film technology

Sina Rouhi [a,b,*], Jose Enrique Martinez-Medina [a], Mehtap Ozdemir [a,c], Mehmet Ertugrul [d], Gulnur Aygun [a], Lutfi Ozyuzer [a,c]

[a] Department of Physics, Izmir Institute of Technology, Urla, 35430, Izmir, Turkey
[b] Department of Nanoscience and Nanoengineering, Ataturk University, 25030, Erzurum, Turkey
[c] Teknoma Technological Materials Inc., Izmir Technology Development Zone, Urla, 35430, Izmir, Turkey
[d] Department of Electric-Electronics, Ataturk University, 25030, Erzurum, Turkey

ARTICLE INFO

Keywords:
Molybdenum boat's lifetime
Thermal evaporation
Continuous feeding

ABSTRACT

The aim of this study is to calculate the optimum lifetime of Molybdenum (Mo) thermal evaporation boats for Copper (Cu) filling in thin film technologies. Three types of Mo boats with thicknesses of 0.2, 0.3 and 0.5 mm were used during the experiments under the high vacuum condition about 6.0×10^{-6} Torr. The behavior of each boat was investigated by focusing on the total amount of evaporation material, operational time and applied power. Prior to the deposition process, material was loaded on the evaporation boat by two methods. In the first method, Cu wire was cut into 1 cm long, then every boat was filled with this amount of Cu material. The second alternative feeding method is to use a wire-feeder step motor, which refills boat with Cu wire during evaporation process. The latter one is very useful for continuous deposition process since there is no need to break the vacuum state. In both methods, however, the number of failures during operations increases after a series of experiments have been taken place because of boat aging. The results of failures have been analyzed by various methods, and it has been observed that thinner boats showed better stability for long time operation by continuous feeding technique.

1. Introduction

Several studies have been highlighted the major importance of thermal evaporation technique (TET) as the basic method in thin film deposition. The history of this method goes back to nearly a half-century used in optics and electronics like thin film transistors, since 1960 and caused the development of metal oxide semiconductor IC in the 1970s. Also, the mentioned technology provides a variety of new materials such as diamond-like carbon (DLC), high-T_c superconductors and is still being developed from day to day. This technique is based on resistive heating, where the material is evaporated by a resistively heated refractory metal filament or boat, such as W, Mo, Ta etc. [1]. The TET is perfect method that frequently used in (III–V) compound semiconductor devices because of smooth and soft deposition rate that prevents substrate surface damage [2]. Also it has to mentioned that the Copper thin films are more efficient choices for solar cell devices like CZTSe components [3]. Several new applications of TET like Copper Indium Diselenide ($CuInSe_2$) semiconductor compound were synthesized near stoichiometric properties for solar cells by high absorption coefficient and electrical stability [4,5]. Beside some photovoltaic researches, the ITO/p-Si heterojuntions contacts thin films deposited in the vacuum by thermal evaporation obtained more amorphous structure and good rectifier property [6]. Additionally, transition metal-oxide thin films like nano-structured WO_3 with high surface roughness used in gas sensors have been developed at relatively low deposition rate causes low power consumption and exhibits high compatibility with signal processing devices [7,8]. Thermal evaporation technique provides the possibility for nanowire coating in O_2 ambient pressure at high temperature such as large-scale coper oxide (CuO) nanowire, or vanadium pentoxide (V_2O_5) layers deposited at room temperature [9,10]. It is also useful for producing single-phase $AgInS_2$ [11]. Also the TET has attracted much attention in recent years due to its ease of manufacture and low production cost in large quantity and high-purity. This method has mentioned for ultralong and uniform-sized like a few nanometers by using powder materials such as SiO for nanowires growth [12]. Some papers reported fabrication process of Nanocrystalline materials used in

* Corresponding author. Department of Physics, Izmir Institute of Technology, Urla, 35430, Izmir, Turkey.
E-mail addresses: sinarouhi@iyte.edu.tr, sina.rouhi@atauni.edu.tr (S. Rouhi).

https://doi.org/10.1016/j.vacuum.2020.109167
Received 22 June 2019; Received in revised form 30 December 2019; Accepted 31 December 2019
Available online 3 January 2020
0042-207X/

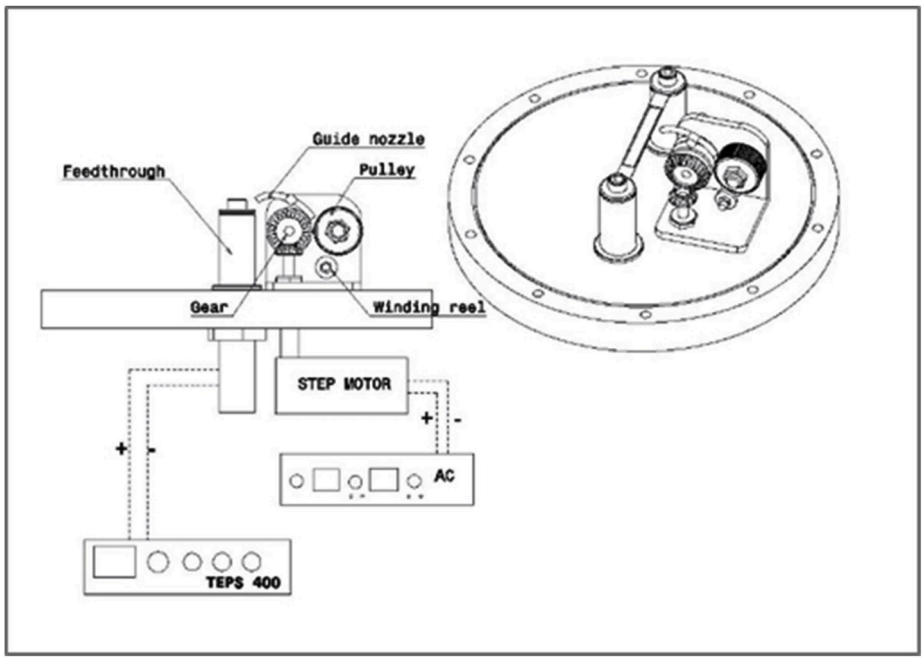

Fig. 1. Wire feeder schematic and sectional descriptions.

Nano-devices like bismuth sulfide thin films were deposited by thermal evaporation technique with sulfide powder as evaporation material [13].

The priority of suitable materials for high-temperature applications is the high melting temperature that causes difficult manufacturing process like casting. Therefore, powder metallurgy technique is a good choice for making molybdenum products with a melting temperature near 2622 °C, but powder sintering temperature is near 2000 °C [14,15] and recrystallization temperature of pure Molybdenum is reported as 1800 °C in (6.7×10^{-4} Pa) [16]. In a short glance, pure Molybdenum shows a good combination of physical properties such as high temperature strength, corrosion resistance, thermal conductivity, high elastic modulus, and a low thermal expansion coefficient, but its important property is weak low temperature ductility. Obviously, recrystallization of Mo leads it to be embrittlement at room-temperature because of impurities such as Nitrogen, Carbon and Oxygen. Recrystallization behavior of Molybdenum influenced by the purity of material and thermo-mechanical treatment process results in some mechanical properties such as ductility and hardness. Moreover, Molybdenum exhibits a high stacking fault energy because of its bcc lattice structure [17]. In this method, it is possible to produce different combined alloy material like Cu_2InO_4 chemically alloyed thin film on silicon substrate under 2×10^{-2} Torr of O_2 gas flow [18]. It should be taken into consideration that thermal evaporation method is used for the evaporation of many metallic materials and is generally useful in device construction. In another study, Zn_2GeO_4, which is a combination of Zn and Ge, is used to preform thermoelectric power generation applications. Zn_2GeO_4 alloy was deposited under constant oxygen gas flow rate on Indium coated glass substrate by evaporation technique [19].

In this study, continuous long-term thin film of at least 1.5 μm thick is required to be obtained. This process is generally used for large-scale roll to roll coatings, and the coating requires a long period of time from start to finish that producing meters of deposited thin film material. Therefore ability to estimate the service-life of boats during process plays an important role in the successful outcome of the project. In addition, in this article, the behavior and possible damages of an important member of thin film deposition family were examined scientifically. The main objective of this research is investigating the molybdenum thermal evaporation boat performance at different thicknesses, for industrial use or continuous coating procedure, because its service life plays an important role in the optimal performance of the boat.

2. Materials and method

2.1. Boat and evaporation metal specifications

The Mo boats, 100×15 mm^2 surface area with 0.2, 0.3 and 0.5 mm thick, have been purchased from Kurt J. Lesker company (PA 15025 USA). Average weights of empty boats' are 0.45, 0.60 and 0.75 g, respectively. The film growth experiments have been carried out in the high vacuum conditions of about (6.0×10^{-6} Torr). A 99.9% pure Copper (Cu) wire was used and its quantity for an operation cycle is a function of the required thickness of the thin film. Cu was loaded into the boats by two methods. First, 1 cm length Cu wire sections were manually loaded into the boat. The average weight of each piece of 1 mm wire diameter is about 0.66 g and the practically calculated maximum loading capacity of the boat is about 5 g. For the second method, the alternative feeding provided by a wire feeder 50 W step motor charges the boat by a long Cu wire during evaporation. The second method is more useful for continuous coating processes like wire/fiber coating on a large scale without breaking the vacuum state. The process results by applying 2 V, then the system loads 1.8 cm (about 1.2 g) in 1 m. Fig. 1 shows the wire feeder scheme.

2.2. Experimental details

An AC power supply (PS) model TEPS-400U is employed for the thermal evaporation process. PS is connected to feedthrough by 300 A cables using cable plugs. Mo boat gradual warming up operation occurs in 5 steps during 2 min intervals. Heating steps comprise the initial current flow, preheating, shining, initial melting and fully melt or boiling.

The primary electrical current is applied to check the electrical contacts and prevents potential damage to the PS as a consequence of current fluctuation. The preheating step avoids any thermal shock to the boat as a result of above operation. Then, since the third stage of heating, thermal radiation is observed from the viewport. During this step, the melting point and turbulence prevention of the molten material is

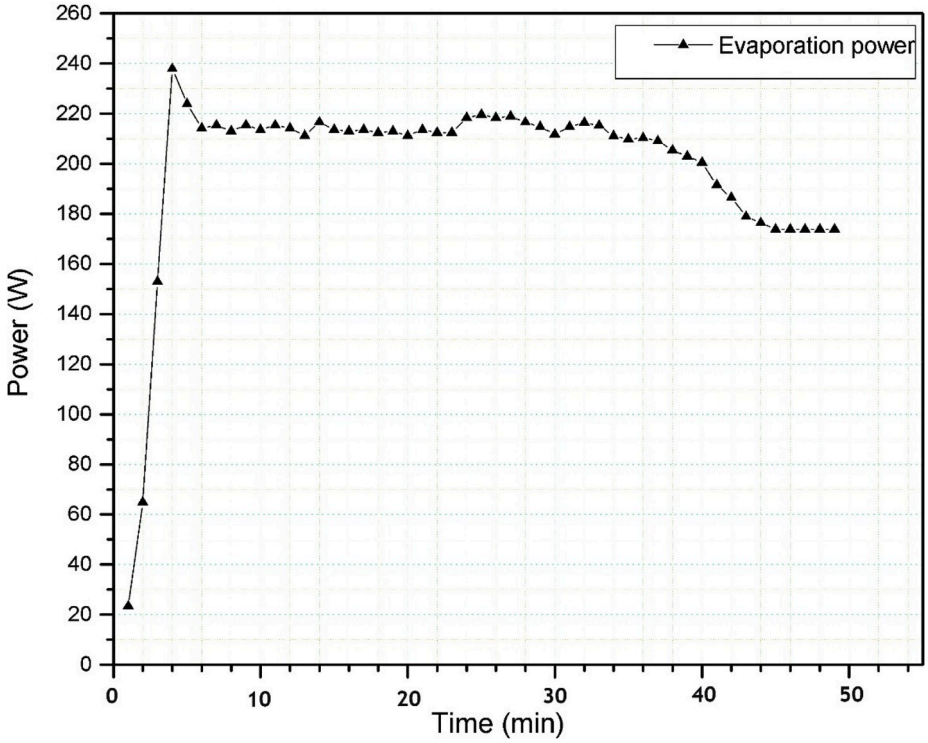

Fig. 2. Typical power ratio changes during thermal evaporation by Mo-0.3 boat.

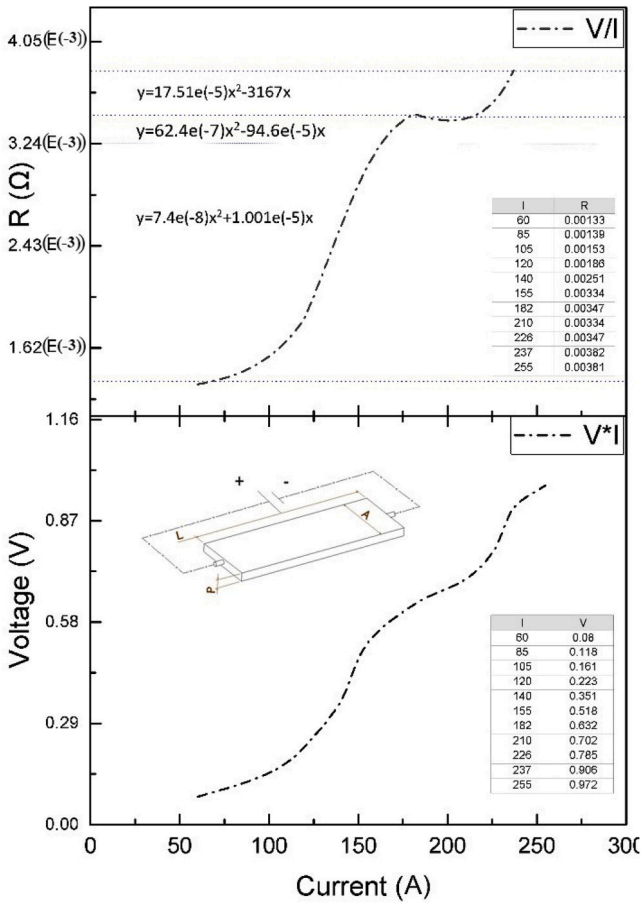

Fig. 3. The specific electrical resistance changes related to electrical current and V/I ratio in Mo-0.3 boat for 5 g of Cu.

observed and controlled. As a consequence of the initial stages, copper wire encounters a slow phase transition and melts from the surrounding. Despite the applied constant voltage, the phase transition causes a drastic increase of electrical current, which results in reaching to the full melting point of the Cu filling. The entire process can be visualized and controlled by the viewport through the full material is evaporated. Moreover, the material's full consumption depends on the boat thickness and is predictable by observing the constant minimum current value. Finally, the current flow gradually reduces to zero. Fig. 2 shows variations in power range during a typical operation by 0.3 mm thick Mo boat.

3. Results and discussion

3.1. Equipment damages

It is well known that if the electric current (I) passes through a resistance (R), it generates electrical power (P) equal to:

$$P = I^2 R \quad (1)$$

The relation between resistance and resistivity (ρ) is given by

$$R = \rho L/A \quad (2)$$

where L is the length of material and A is the cross section. Resistivity of copper and molybdenum is reported as (1.68×10^{-8}) and (5.34×10^{-8}) (ohm.m) at room temperature. The direction of current flow is shown in Fig. 3. According to (1) and (2), electrical resistance (R) and consequently generated power will decrease by increasing the boat thickness [20]. Consequently, in order to prevent temperature drop, the resistance reduction in the process must be compensated by increasing the current. As consequence of the constant resistance of the cables, the higher current flow most probably causes an increment of the internal temperature of cable and burn it from the connection area. In addition, when an excess current is supplied, it causes to warm up the power supply. As the deposition process stops when the cable burns during the operation, the frozen residual Cu pieces may remain inside the boat as a

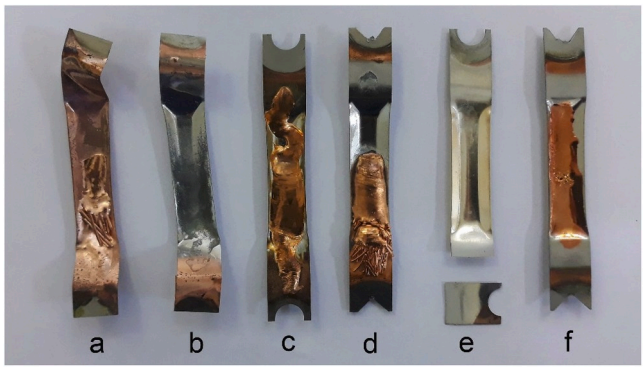

Fig. 4. The boat failure types: (a) Mo-0.2 boat deformation and half heated boat, (b) Mo-0.2 boat deformation and local degradation, (c) Mo-0.3 conductive boat, (d) Mo-0.3 half heated boat, (e) Mo-0.5 boat brittleness and fracture and (f) Mo-0.5 equipment damage and operation aborting.

consequence, resulting in cracks and lateral damages. Fig. 3 shows V/I ratio during a single operation for 5 g of copper from 0.3 mm thick Mo boat. As it is seen, increment in current flow causes an increase in specific electrical resistance of Mo boat and, consequently, increment of the equipment's warming ratio.

Fig.s 4 and 5 illustrate the macroscopic and microscopic combined images of the problems observed about the boat group, which will be explained in related sections. Fig. 4 exhibits boat deformation and local degradation of Mo-0.2 half heating damage, of Mo-0.2 and Mo-0.3, surface conductivity of Mo-0.3, also Mo-0.5 boat brittleness fracture and equipmental damage and operation aborting. Also Fig. 5 shows optical microscope images of uniform corrosion, grain boundaries erosion-corrosion, Cu/Mo intersection, local erosion in half heated boat and the copper movement to the contacts that cause to electrical conductivity.

3.2. Half-heated boat

According to the relationship between sheet thickness and resistivity given in equation (2), local erosion of the boat surface increases the electrical resistance of the cross-section which causes heterogeneous current flow and inappropriate heat distribution. This causes sectional heating and, as a result, partial melting. Consequently, by increasing the molten metal's kinetic energy on the hot side, the half solid metal is pushed to the other side to decrease the turbulence level. As a result of metal condensation, the cross-section of the cold part increases and the electrical resistivity of that part decreases. This phenomenon results in a complete damage of the boat and aborts the operation. Fig. 4(a) and 4(d) show the half heated boat that has three parts as fully solid, just melted and evaporated regions. Besides, Fig. 4(f) shows an aborted operation along with residual material inside the boat. Because of these technical reasons, this boat will not be used again in future growth processes. Fig. 5(d) shows an optical microscope image of local erosion nearly the center of the boat that causes heterogeneous heating.

3.3. Conductive boat

The surface roughness of the materials is responsible for the wettability ratio. Wettability is defined as the observed contact angles between solid-liquid interface and heterogeneous rough surface which shows a wider contact angle. According to Wenzel theory, it describes the rough surface extension in comparison to the smooth surface, where the maximum contact angle (θ) has to be $0^\circ < \theta < 90^\circ$ [21]. On the other hand, Cassie-Baxter theory investigated an apparent contact angle equation for the heterogeneous contact between a liquid droplet and a composite surface that (f) is the area fraction and (1-f) shows air consumption on area, which is:

$$\cos\theta = f\cos\theta_0 - (1\text{-}f) \tag{3}$$

In the formula, θ_0, is a flat solid surface contact angle with a liquid droplet [22]. The homogenous surface crack and the erosion-corrosion cause topographical changes and intersections of grain boundaries with the boat surface. This phenomenon increases the contact angle (θ) between the liquid metal and the surface. Also, the high kinetic energy of molten metal allows the dispersion of the liquid mass. The grain boundaries tension (γ_{GB}) will continue up to reach a vectorial equilibrium to the surface tension (γ_s) of the boat [23]. Therefore, the molten metal flows into contacts for minimizing the turbulence and results in conductivity and failure of the boat. Equation (4) shows the relationship between tension forces:

$$\gamma_{GB} = 2\,\gamma_s.\cos(\theta) \tag{4}$$

Fig. 4(c) and 5(c) show the macro and microscopic images of conductive boat respectively with a conductive Cu line between the contacts on the boat surface [23]. Fig. 5(e) shows the copper droplets directly aligned to the contacts.

3.4. Boat deformation

Polycrystalline materials are influenced by grain boundaries (GB) to minimize the Gibbs energy by planar segregation and strongly affect the bulk properties of the material. The impurities in commercially pure materials also drastically affect the kinetic properties of the interfaces. Equation (5) determines GB diffusivities as in the following formula:

$$P = \delta.\, D_{GB} \tag{5}$$

where δ is the GB width and D_{GB} is the GB diffusion coefficient respectively [24]. One of the main reasons for more grain boundary mobility is

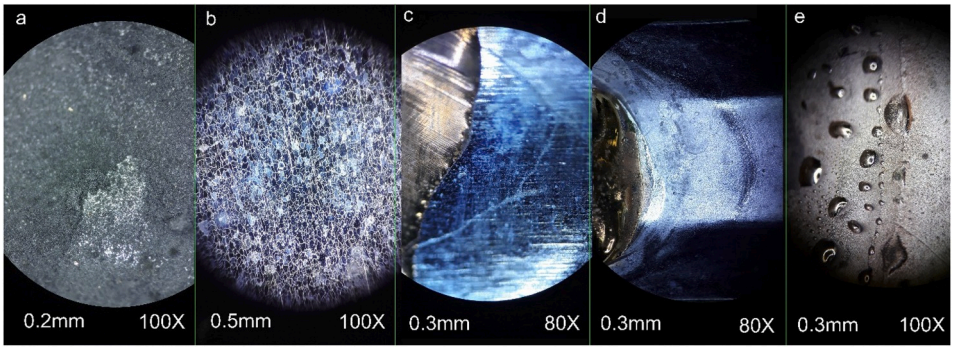

Fig. 5. Optical microscope images of boat failures. (a) Mo-0.2 boat by uniform corrosion, (b) Mo-0.5 boat grain boundaries erosion-corrosion, (c) Mo-0.3 boat Cu/Mo intersection in conductive boat failure, (d) the local erosion in half heated boat and (e) the copper droplets directed to the contacts and cause to electrical conductivity.

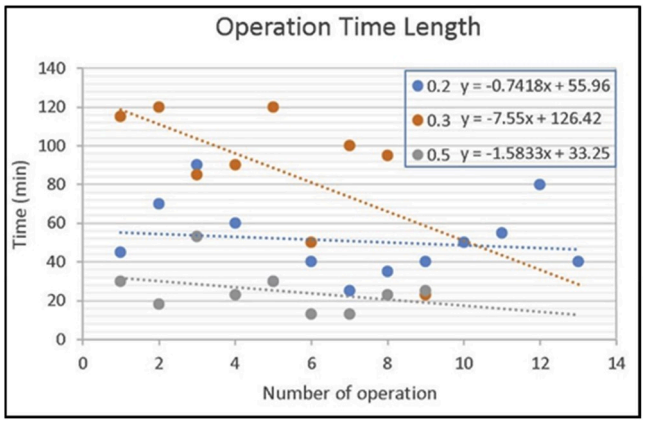

Fig. 6. The operating time changes in 1.2 (V) related to boat aging using a constant mass for 5 g.

the low amount of impurity content in the material structure. However, the grain size causes a 5–20% deformation [17]. Also, according to another research, the linear elongation for Mo is 0.4–0.6% of the size between 1000 and 1400 K [25]. The thermal expansion of molybdenum has been determined between 1100 K and 2500 K. Metal exhibits a uniform thermal expansion over the temperature range increasing by flowing quadratic equations.

$$a / a_0 = 0.987 \times 10^{-3} + 2.40 \times 10^{-6}(T - 273) + 2.20 \times 10^{-9}(T - 273)^2 \quad (6)$$

In this formula, a_0 is the lattice parameter and a is the lattice parameter after deformation [26]. Deformation occurs more often in the thinner boats because of low impurity range and low amount of (δ) and also low kinetic energy of GB diffusion (P). Therefore, due to the boat is fixed to the feedthroughs, thermal expansion causes plastic deformation. This undesired deformation leads liquid to drown out or molten metal concentration and the local erosion on the boat surface. Fig. 4(a) and 4 (b) exhibit boat deformation and Fig. 5(a) shows a microscopic image of the uniform corrosion due to the molten metal concentration.

3.5. Brittle boat

Due to discontinuous operation, boats are faced to be ductile as a result of brittle phase transition. Moreover, increasing the operating temperature about the molybdenum annealing range leads to the boat's low-temperature brittleness because of bcc structure of Molybdenum [17]. The main reason of fragility is the movement of dislocations towards the grain boundaries and, consequently, further hardness. Annealing temperature for molybdenum has been reported as about 1300 °C [27]. According to some operational reports and the reference

Table 1
The possibility of failure for each boat, related to the thickness that I < II < III.

Damage factor	0.2	0.3	0.5
Degradation	II	III	I
Fragility	I	II	III
Half-heated	I	II	III
Electrical conductivity	I	III	II
Deformation	III	II	I
Equipment damage	I	II	III
Max. operational power	I	II	III

data, Cu melting point under vacuum conditions (10^{-6} Torr) is about 852 °C [28]. Therefore, the operating temperature in vacuum conditions is not sufficient for recrystallization and structural repair. Since surface corrosion causes local thickness decreasing, and creating a stress concentration zone, it leads to fracture of the boat from the poorest mechanical contact. Moreover, because of the existence of a cooling system probably after cutoff the current, rapid cooling occurs resulting in a metallurgical quenching and increasing the hardness of the boat. After several operations, any mechanical effect can easily damage and break the boat. According to Buchanovsky et al. the cold brittleness temperature increases, if the boat is annealed about 2000 °C because of grain growth [29]. Fig. 4(e) shows the broken boat due to mechanical stress after the heating operation.

3.6. Evaporation rate of constant evaporation material for various boats

As a result of vacuum condition below 10^{-6} Torr any kinds of oxidation is not noticeable but the final evaporation time for the 5 g of material at lower vacuum ranges is even lower. According to obtained data, the average evaporation time in 5.0×10^{-6} Torr and 8.0×10^{-6} Torr of vacuum condition known as 30 and 35 min, respectively. Also, lower vacuum levels result in more scattering of the vapor atoms and formation of a heterogeneous topography on the substrate. According to data analysis, the average operating time for constant mass of material is affected by operation parameters and decreases with a specific slope by boat aging. Fig. 6 shows the changes in the operating time related to aging by applying about 1.2 V of constant voltage that was observed for different thicknesses.

3.7. Operational power ratio changes related to boat lifetime and maximum load capacity

Average power required for various stages of operation increases with a gentle slope with respect to the boat aging. Besides, this slope increases by increasing boat thickness because of higher grain boundaries and more intergranular cracks. Moreover, regarding the discussions in sections (3.1), (3.4) and (3.5), total amount of material

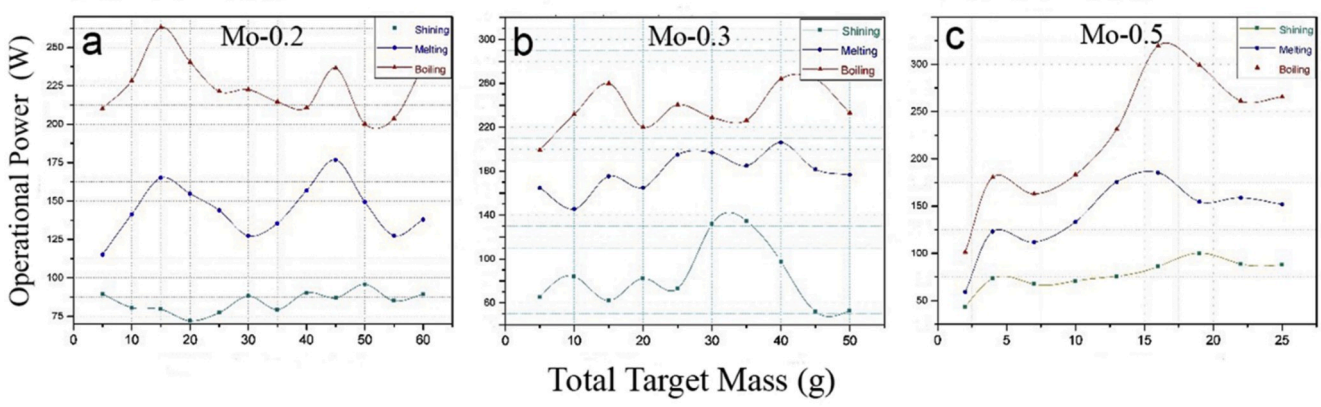

Fig. 7. The operational power changes by total amount of metal load.4(a): Mo-0.2, 4(b): Mo-0.3 and 4(c): Mo-0.5 mm.

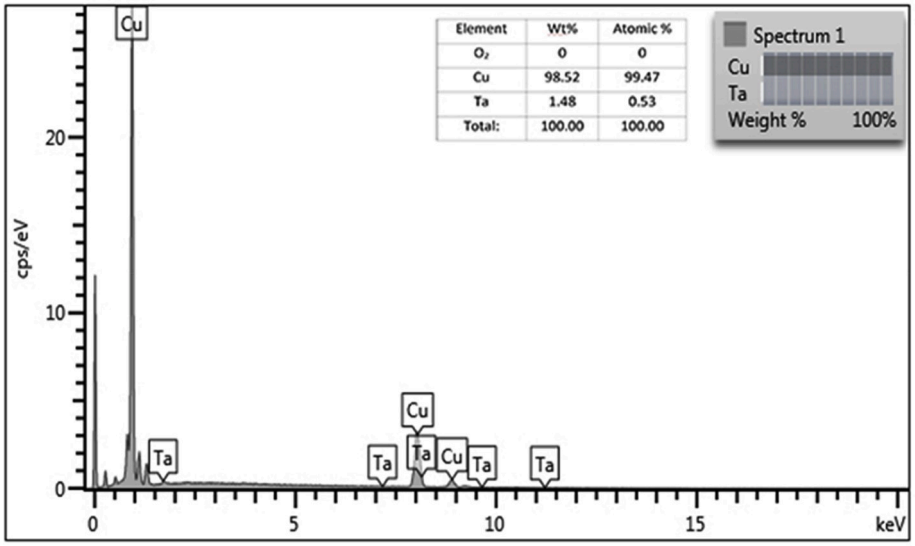

Fig. 8. EDX analysis of deposited Copper chemical composition on Tantalum coated surface.

decreases because of disruption in operation system for thicker boats with a shorter life time. Fig. 7 shows the operational power changes and the total mass of material during the lifetime for various boat types. The analysis consists of three stages, which show the thermal radiation (shinning), melting and boiling of the material. As a result of boat aging related research, the required power for each stage increases on average. The more power range increment is the more tangible for thicker boats. Fig. 7(a), (b) and (c) exhibit 0.2, 0.3 and 0.5 mm thick boats operational performance, respectively. As shown in Mo-0.2, the boat service life is higher than others according to maximum material mass and the average of working performance relied on applied power is progressing steadily in compare of Mo-0.5.

3.8. Observed damage possibility related to boat thickness

Regarding experimental observations based on gathered data, there is some possibility of damage for boat variations related to the thickness. Some of failure types more often observed related to boat structure. These possibility ranges showed by I for the lowest and III for the highest observation. The boats with a thickness of 0.2 mm generally show the lowest physical damage and by increasing the thickneses, possibility of damage increases in operating systems. Damages have been grouped in Table 1. indicating the damage possibility for boat groups.

3.9. The chemical composition observations of thermally evaporated copper

This method allows to produce large quantities of products based on continuous coating and use them throughout the industry in several micron like Copper thin film deposition on PET and textile or on a coated surface. Thanks to the high vacuum, it provides the minimum oxide in copper structure (about zero). There is an example of EDX analysis can be seen as given in Fig. 8 about deposited Copper chemical composition on Tantalum coated surface. It apparently shows the 0% of oxidation inside structure.

4. Conclusions

According to the results, it is better to consider the total amount of material mass as the scale of boat life instead of operation time under high vacuum condition about 6.0×10^{-6} Torr, because of more reasonable and accurate obtained results. The present research exhibited 8 types more often faced damages grouped as degradation, fragility, half-heated, electrical conductivity, deformation, equipment damage and maximum operational power about Mo boats related to their thickness and mass inside high vacuum state. Mo-0.2 coded boat group shows better elasticity despise of mechanical stress but their structure is very capable to plastic deformation. Degradation is a common phenomenon in Mo-0.3 boats also they commonly face to electrical conductivity on surface due to Cu condensation. Despite of all estimates the Mo-0.5 boats are not comfortable to continue using because of lower electrical resistance in compare of Mo-0.2 that causes to lower deposition performance. According to the present test condition, a thinner boat exhibits more stability, but the limitations of cooling/heating frequencies can exhibit better performance and continuous deposition maybe avoid the frequently occurred thermal shocks and physical damages. Also, decreasing the cable's electrical resistance by increasing diameter will cause more stability for thicker boats.

Acknowledgments

The authors would like to acknowledge the characterization facilities used in Applied Quantum Research Center (AQuReC) of Izmir Institute of Technology for the current study.

References

[1] H. Adachi, K. Wasa, Thin Films and Nanomaterials, Handb. Sputter Depos. Technol. Fundam. Appl. Funct. Thin Film. Nano-Materials MEMS, second ed., 2012, pp. 3–39, https://doi.org/10.1016/B978-1-4377-3483-6.00001-2.
[2] G.J. Burek, Y. Hwang, A.D. Carter, V. Chobpattana, J.J.M. Law, W.J. Mitchell, B. Thibeault, S. Stemmer, M.J.W. Rodwell, Influence of gate metallization processes on the electrical characteristics of high-k/In0.53Ga0.47As interfaces, J. Vac. Sci. Technol. B, Nanotechnol. Microelectron. Mater. Process. Meas. Phenom. 29 (2011), 040603, https://doi.org/10.1116/1.3610989.
[3] M.A. Olgar, Y. Atasoy, B.M. Başol, M. Tomakin, G. Aygun, L. Ozyuzer, E. Bacaksiz, Influence of copper composition and reaction temperature on the properties of CZTSe thin films, J. Alloy. Comp. 682 (2016) 610–617, https://doi.org/10.1016/j.jallcom.2016.04.309.
[4] N.M. Shah, C.J. Panchal, V.A. Kheraj, J.R. Ray, M.S. Desai, Growth, structural and optical properties of copper indium diselenide thin films deposited by thermal evaporation method, Sol. Energy 83 (2009) 753–760, https://doi.org/10.1016/j.solener.2008.11.006.
[5] N.M. Shah, J.R. Ray, K.J. Patel, V.A. Kheraj, M.S. Desai, C.J. Panchal, B. Rehani, Structural, electrical, and optical properties of copper indium diselenide thin film prepared by thermal evaporation method, Thin Solid Films 517 (2009) 3639–3644, https://doi.org/10.1016/j.tsf.2008.11.133.
[6] A. Ozkartal, Characterization of the ITO/p-Si/Al contacts produced by thermal evaporation, Vacuum 168 (2019), 108799, https://doi.org/10.1016/j.vacuum.2019.108799.

[7] S. Li, Z. Yao, J. Zhou, R. Zhang, H. Shen, Fabrication and characterization of WO 3 thin films on silicon surface by thermal evaporation, Mater. Lett. 195 (2017) 213–216, https://doi.org/10.1016/j.matlet.2017.02.078.
[8] A. Ponzoni, E. Comini, M. Ferroni, G. Sberveglieri, Nanostructured WO3 deposited by modified thermal evaporation for gas-sensing applications, Thin Solid Films 490 (2005) 81–85, https://doi.org/10.1016/j.tsf.2005.04.031.
[9] L.S. Huang, S.G. Yang, T. Li, B.X. Gu, Y.W. Du, Y.N. Lu, S.Z. Shi, Preparation of large-scale cupric oxide nanowires by thermal evaporation method, J. Cryst. Growth 260 (2004) 130–135, https://doi.org/10.1016/j.jcrysgro.2003.08.012.
[10] R. Santos, J. Loureiro, A. Nogueira, E. Elangovan, J.V. Pinto, J.P. Veiga, T. Busani, E. Fortunato, R. Martins, I. Ferreira, Thermoelectric properties of V 2 O 5 thin films deposited by thermal evaporation, Appl. Surf. Sci. 282 (2013) 590–594, https://doi.org/10.1016/j.apsusc.2013.06.016.
[11] Y. Akaki, S. Kurihara, M. Shirahama, K. Tsurugida, S. Seto, T. Kakeno, K. Yoshino, Structural, electrical and optical properties of AgInS2 thin films grown by thermal evaporation method, J. Phys. Chem. Solids 66 (2005) 1858–1861, https://doi.org/10.1016/j.jpcs.2005.09.005.
[12] Z.W. Pan, Z.R. Dai, L. Xu, S.T. Lee, Z.L. Wang, Temperature-controlled growth of silicon-based nanostructures by thermal evaporation of SiO powders, J. Phys. Chem. B 105 (2001) 2507–2514, https://doi.org/10.1021/jp004253q.
[13] K. Mageshwari, R. Sathyamoorthy, Influence of substrate temperature on the physical properties of thermally evaporated nanocrystalline bismuth sulfide thin films, Vacuum 86 (2012) 2029–2034, https://doi.org/10.1016/j.vacuum.2012.04.006.
[14] C. Colombo, M. Heiβ, M. Grätzel, A.F. Morral, C. Colombo, M. Hei, M. Grätzel, A. F. Morral, Gallium Arsenide Radial Structures for Photovoltaic Applications, 2010, pp. 2007–2010, https://doi.org/10.1063/1.3125435, 173108.
[15] D.C. Blaine, J.D. Gurosik, S.J. Park, D.F. Heaney, R.M. German, Master sintering curve concepts as applied to the sintering of molybdenum, Metall. Mater. Trans. A Phys. Metall. Mater. Sci. 37 (2006) 715–720, https://doi.org/10.1007/s11661-006-0043-9.
[16] Y. Hiraoka, H. Kurishita, M. Narui, H. Kayano, Fracture and ductile-to-brittle transition characteristics of molybdenum by impact and static bend tests, Mater. Trans., JIM 36 (2014) 504–510, https://doi.org/10.2320/matertrans1989.36.504.
[17] S. Primig, H. Leitner, H. Clemens, A. Lorich, W. Knabl, R. Stickler, On the recrystallization behavior of technically pure molybdenum, Int. J. Refract. Metals Hard Mater. 28 (2010) 703–708, https://doi.org/10.1016/j.ijrmhm.2010.03.006.
[18] J. Jacob, R. Wahid, A. Ali, R. Zahra, S. Ikram, N. Amin, A. Ashfa, U. Rehman, S. Hussain, D.S. Al-Othmany, S.Z. Ilyas, K. Mahmood, Growth of Cu 2 InO 4 thin films on Si substrate by thermal evaporation technique and enhancement of thermoelectric properties by post-growth annealing, Phys. B Condens. Matter 562 (2019) 59–62, https://doi.org/10.1016/j.physb.2019.03.023.
[19] R. Zahra, K. Mahmood, A. Ali, U. Rehman, N. Amin, M.I. Arshad, S. Hussain, M.H. R. Mahmood, Growth of Zn2GeO4 thin film by thermal evaporation on ITO substrate for thermoelectric power generation applications, Ceram. Int. 45 (2019) 312–316, https://doi.org/10.1016/j.ceramint.2018.09.168.
[20] E. Bogatin, Prentice Hall Modern Semiconductor Design Series, Prentice Hall signal integrity library, 2010.
[21] K.J. Kubiak, M.C.T. Wilson, T.G. Mathia, P. Carval, Wettability versus roughness of engineering surfaces, Wear 271 (2011) 523–528, https://doi.org/10.1016/j.wear.2010.03.029.
[22] V. Belaud, S. Valette, G. Stremsdoerfer, M. Bigerelle, S. Benayoun, Wettability versus roughness: multi-scales approach, Tribol. Int. 82 (2015) 343–349, https://doi.org/10.1016/j.triboint.2014.07.002.
[23] S. Kehrein, Modern Developments, 2006, https://doi.org/10.1007/3-540-34068-8_5.
[24] D. Prokoshkina, V.A. Esin, G. Wilde, S.V. Divinski, Grain boundary width, energy and self-diffusion in nickel: effect of material purity, Acta Mater. 61 (2013) 5188–5197, https://doi.org/10.1016/j.actamat.2013.05.010.
[25] I.K. Suh, H. Ohta, Y. Waseda, High-temperature thermal expansion of six metallic elements measured by dilatation method and X-ray diffraction, J. Mater. Sci. 23 (1988) 757–760, https://doi.org/10.1007/BF01174717.
[26] J.W. Edwards, R. Speiser, H.L. Johnston, High temperature structure and thermal expansion of some metals as determined by x-ray diffraction data. I. Platinum, tantalum, niobium, and molybdenum, J. Appl. Phys. 22 (1951) 424–428, https://doi.org/10.1063/1.1699977.
[27] C.L. Briant, H.J. Grabke, Grain boundary segregation in iron and its alloys and its effect on intergranular fracture, Mater. Sci. Forum 46 (2009) 253–276. https://doi.org/10.4028/www.scientific.net/msf.46.253.
[28] V. Level, C. Temperature, C. Type, E.C. Type, P. Choices, L. Temp, O. Al, H. Temp, Evaporation Guide for the Elements, 2008, 2008.
[29] V. V Buchanovsky, I. Mamuzi, E.P. Polishuk, The effect of heat treatment on mechanical characteristics and nature of failure of sheet molybdenum alloys, Metalurgija 46 (2007) 233–236.